CERN's SUMMER STUDENT PROGRAMME 2024

Evaluation of the β-particle detection performance at DeVITO

Student: Raluca-Andreea Miron (University of Bucharest)

Supervisors: Monika Piersa-Siłkowska (CERN), Ilaria Michelon (CERN, Univ. of Geneva)

30 August 2024

Abstract

During the Summer Student Programme at CERN, I worked on a project at the ISOLDE facility. The project focused on evaluating the β-particle detection performance of β-particle detectors within the DeVITO spectroscopy station at the VITO beamline. The commissioning run at DeVITO was performed in July 2023, and it was followed by the first physics experiment in April 2024. These two online runs were conducted with different setup geometries, resulting in different instrumental responses. To investigate the β-particle detection performance for radiation emission asymmetry measurements, we carried out Monte Carlo simulations. These simulations investigated the detectors' response to electrons of varying energies, including detection efficiency and energy deposition in the different setup components.

1 Introduction

1.1 DeVITO end station

β-decay spectroscopy is a powerful technique for studying the properties of radiation emitted from atomic nuclei, enabling the observation of excited states and providing valuable insights into their nuclear structure. In conventional β-decay experiments, there is a limited ability to deduce spins and parities of states [1]. This limitation can be overcome using spin-oriented nuclei [2]. The VITO beamline [3] for laser-induced polarisation of radioactive beams at ISOLDE is a suitable place to adopt this novel technique.

DeVITO is a new end-station for β-decay spectroscopy with laser-polarised beams, which was integrated into the VITO beamline. The detection setup consists of β-particle, γ-ray, and neutron detectors to measure the radiation emitted from laser-polarised unstable nuclei. Two β-particle detectors used to measure β-particle emission asymmetry are the main focus of the Summer Student Project. These detectors are located in the experimental chamber, where radioactive nuclei are implanted into a host crystal positioned in the centre of the chamber.

The commissioning run at DeVITO [4] was conducted in July 2023 and it was followed by the first physics experiment in April 2024. The second online run featured several upgrades compared to the initial 2023 setup. These improvements included a new front β-particle detector with a larger aperture to enhance beam transmission and a different geometry of the implantation crystal. The following sections discuss the effects of these changes on the β-particle detection performance.

1.2 β-particle detector assembly

The β-particle detector assembly is positioned at the centre of the main chamber, enclosed within a compact magnet. In this setup, two plastic scintillator detectors are placed at 0° and 180° angles with respect to the beam polarisation axis, and a cubic crystal is situated in the middle of the two, serving as the implantation host.

During the 2023 commissioning experiment, the detectors consisted in a 6.3-mm thick EJ200 plastic scintillator with a 10 mm circular aperture, and a 0.5 mm KCl crystal was used as implantation host. However, after the upgrades of the 2024 experiment, the front detector was replaced with a 5-mm thick EJ204 plastic scintillator with a 20 mm aperture, and the previous implantation host was substituted with a 2-mm thick crystal. Table 1 presents the main properties of the detectors and implantation hosts used in two online runs. Different geometry configurations result in different instrumental responses that are inherent in two setups.

Design	2023	2024
Back detector	EJ 200	EJ 200
Front detector	EJ 200	EJ 204
Aperture	10 mm	20 mm
Back detector thickness	6.3 mm	6.3 mm
Front detector thickness	6.3 mm	5 mm
KCl diameter	12 mm	20 mm
KCl thickness	0.5 mm	2 mm

Table 1: Parameters for the β-detector geometries.

2 Geant4 simulations

Geant4 (GEometry-ANd-Tracking) is a Monte Carlo toolkit developed and maintained at CERN, designed to simulate the passage of particles in matter, utilizing Monte Carlo methods [5].

The development of the simulation code was carried out in several steps. The class `G4UserPhysicsList` defines the relevant electromagnetic interactions specific to our case. The particle source, along with its associated properties—such as energy distribution, direction, type, and creation vertex—is specified in the class `G4UserPrimaryGeneratorAction`. Additionally, the physical setup, including the definition of materials, their properties, and their arrangement, is defined using Geant4's `G4VUserDetectorConstruction` class. Geant4 allows certain regions of the detector to be designated as sensitive detectors, enabling the recording of simulation results, which are then stored using the ROOT toolkit.

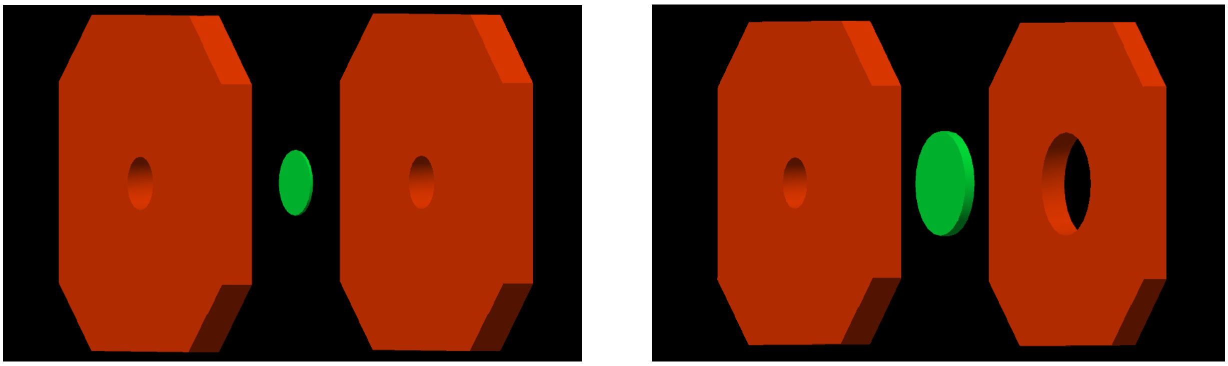

Figure 1: Geometries of the detector setup implemented in Geant4 code.

In this work, a geometrical model of the β-particle detectors and implantation hosts was implemented using Geant4. Figure 1 illustrates the two different configurations (see Table 1) which were simulated.

3 Results and discussions

The aim of the simulations is to assess the response of the β-particle detectors to electrons emitted isotropically from the surface of the crystal. To achieve this, we used mono-energetic beams of 10^6 electrons ranging from 0.1 to 14 MeV, implemented with the `G4ParticleGun`. Additionally, we simulated realistic β-particle energy spectra of radioactive isotopes using `G4GeneralParticleSource`. The goals are to calculate the detection efficiency, study the energy deposition in the detectors and implantation host, and investigate the instrumental asymmetry, which is defined as the difference in counts registered in the front and back detectors normalised by the sum of counts in these two detectors.

3.1 Mono-energetic electron beams

Figures 2a and 2b show the detection efficiency as function of incident energy for the commissioning and first physics experiments, respectively. In the 2023 geometry, at low energies, the back detector registers very few counts because the electrons are primarily stopped by the crystal. However, as the energy increases, electrons manage to pass through the crystal volume and reach the back detector. At high energies, the crystal's influence on the asymmetry response is not significant anymore. In the 2024 geometry, a similar trend is observed at low energies up to 1 MeV, until the electrons have energy sufficient to escape from the crystal volume. At higher energies, the efficiency has similar values to the first case, although the front detector exhibits lower efficiency due to the reduced surface of interaction.

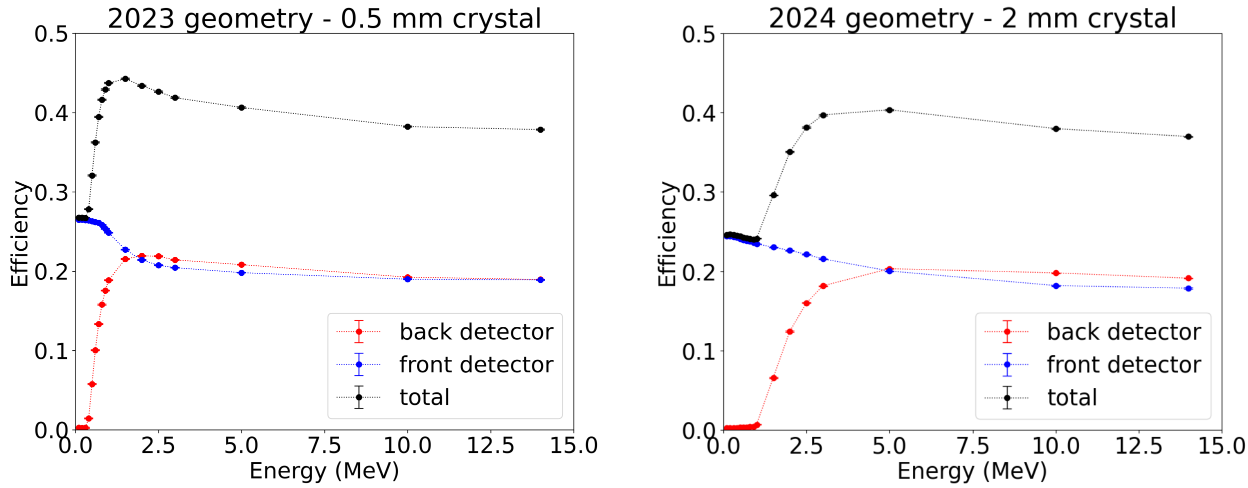

(a) (b)

Figure 2: The detection efficiency as function of incident β-particle energy for the simulated detectors.

In Figure 3a and 3b, each curve represents the energy deposition in the back detector as a function of energy for different incident beam energies. For the 2023 geometry, it can be observed that there are few counts in the low-energy range (top panel) because the electrons are partially absorbed by the implantation crystal. As the incident energy increases (middle panel), the energy deposition curve begins to exhibit a Bragg-like behavior, with a maximum of counts at around 1.5 MeV. Additionally, for energies above 5 MeV, the curves overlap, confirming that the crystal does not significantly influence the detectors' response at high energies. According to Nucleonica database [6], 2 MeV electrons can be stopped by 6 mm of KCl crystal and 10 mm of EJ 200 scintillator.

For the 2024 geometry, the counts are much lower than those in the 2023 configuration for the same incident energies. This is due to the increased thickness of the crystal (2 mm), which results in greater absorption of electrons. Looking at the medium energy range panels, we observe that the curves become broader and less distinct compared to the previous setup. This broadening is attributed to the increased energy loss processes occurring within the crystal, such as scattering and partial absorption, which contribute to a more smeared-out energy spectrum. Similar to the 2023 plot, the high-energy electrons produce overlapping curves, indicating that the crystal produces no effects upon the deposited energy distribution above 5 MeV.

It is advantageous that both geometries exhibit similar behavior at high energies, as our focus is on very neutron-rich nuclei, which emit highly energetic β-particles.

3.2 Relevant β-decay spectra

The selection of neutron-rich potassium isotopes ^{47}K ($Q_\beta = 6.6$ MeV), ^{49}K ($Q_\beta = 11.6$ MeV), and ^{51}K ($Q_\beta = 13.8$ MeV) for the commissioning experiment is motivated by their abundant production at ISOLDE, which compensates for lower detection efficiency when measuring β-decay asymmetry in coincidence with delayed radiation [4]. Heavier isotopes, ^{49}K and ^{51}K, are ideal for β-delayed neutron studies, as their neutron emission spectra provide distinct lines for analysing β-decay transitions, enabling the determination of spins and parities of excited states using the method developed by a group from the University of Osaka [2]. The β-particle spectra of the three isotopes are displayed in Figure 4.

Figures 5a and 5b show the detection efficiency for each simulated isotope spectrum using the 2023 and 2024 geometries, respectively. In the first figure, the efficiency values for the front and back detectors are

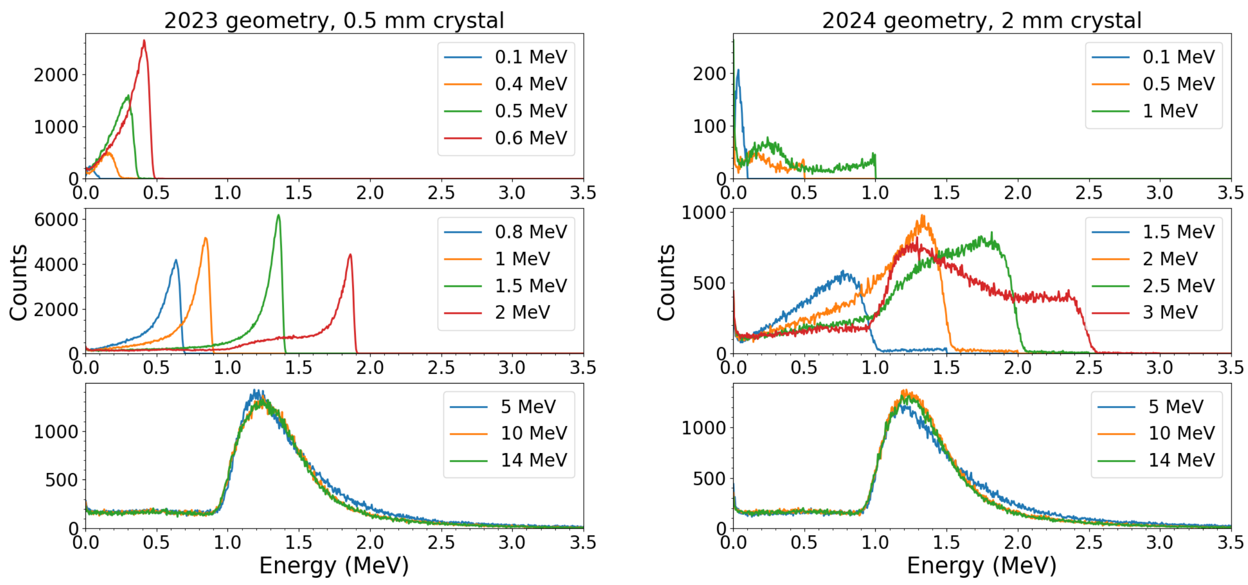

(a) (b)

Figure 3: The energy deposition curves as function of incident energy corresponding to the back detectors in each simulated geometry.

nearly identical for all β-spectra, which is expected given that the detectors have the same dimensions and the KCl crystal used for implantation is very thin. However, in the 2024 geometry, with different detectors and a thicker implantation host, the detection efficiencies differ significantly between the front and back detectors, with efficiency increasing at higher energies, particularly for ^{51}K.

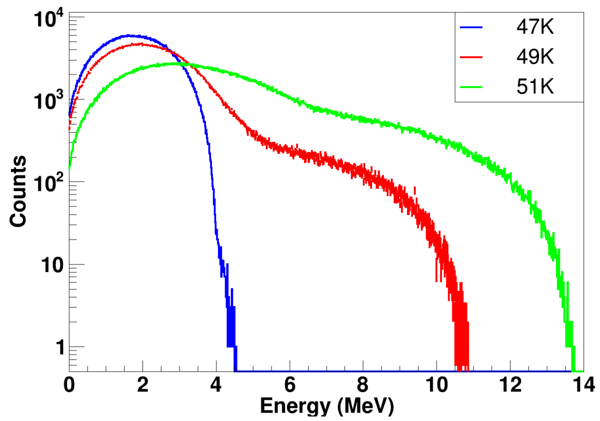

Figure 4: Simulated β spectrum of K isotopes of interest.

Figure 6 presents a series of simulations depicting the energy deposited by β-particles in the front and back detectors (top), along with the associated instrumental asymmetry plot (bottom).

Figures 6a, 6c and 6e show results obtained for the 2023 geometry, where the energy deposition curves for both detectors are very similar. Significant difference is observed at electron energies below 1 MeV, where some β-particles are absorbed in the KCl crystal and cannot reach the back detector. The instrumental asymmetry exhibits a flat behavior as a function of energy for all simulated isotopes.

Figures 6b, 6d and 6f present results from the 2024 geometry, where significant differences in counts are observed between the front and back detectors. In the case of ^{47}K, with an average Q_β energy of 1.8 MeV, the back detector registers a lower count rate across all energy ranges compared to the front detector, indicating that with the 2 mm crystal, more β-particles are absorbed or scattered before reaching the back detector. For ^{49}K (average Q_β = 2.5 MeV), the two curves begin to overlap at higher energies, as electrons gain sufficient energy to pass through the crystal.

However, in the case of the ^{51}K isotope, with an average Q_β energy of 4.2 MeV , the difference between the front and back detectors is more pronounced. The front detector exhibits a sharper peak around 1 MeV, with a higher count rate than the back detector up to this threshold, reflecting the attenuation effects of the thicker crystal. Beyond this point, the energy deposition in the back detectors starts to increase, and at higher energies, the back detector registers more counts than the front detector. This is due to the larger interaction volume in

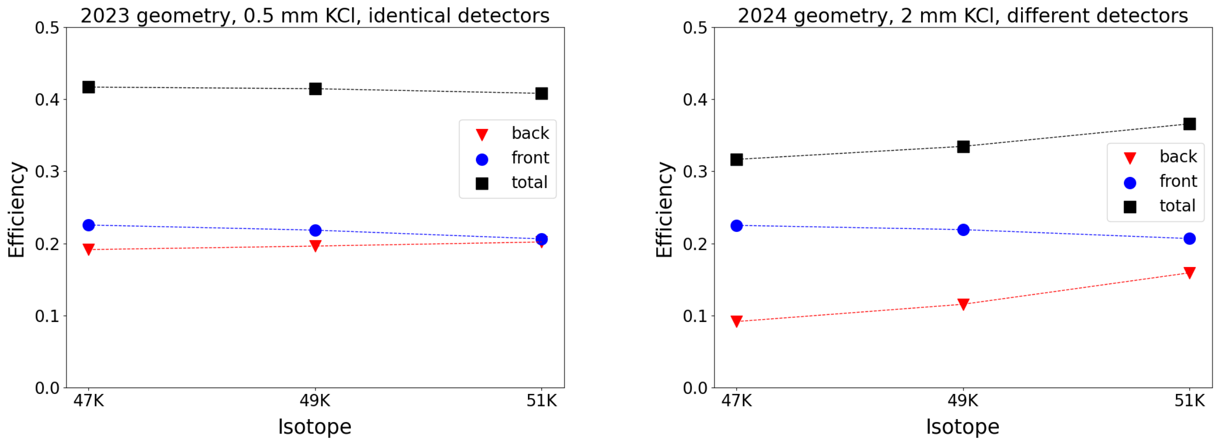

(a) (b)

Figure 5: Detection efficiency for each detector obtained by simulating β spectra of neutron-rich K isotopes.

the back detector, which has a 10 mm aperture, compared to the 20 mm aperture of the front detector, allowing it to capture more high-energy β-particles.

The energy dependence of the instrumental asymmetry is more evident in the 2024 setup, due to different detector characteristics and different crystal thicknesses. In most cases, we observe a positive asymmetry, indicating more counts in the front detector. However, an exception is seen with the ^{51}K isotope, where the back detector, due to its larger interaction surface, records more counts than the front detector, resulting in a negative asymmetry.

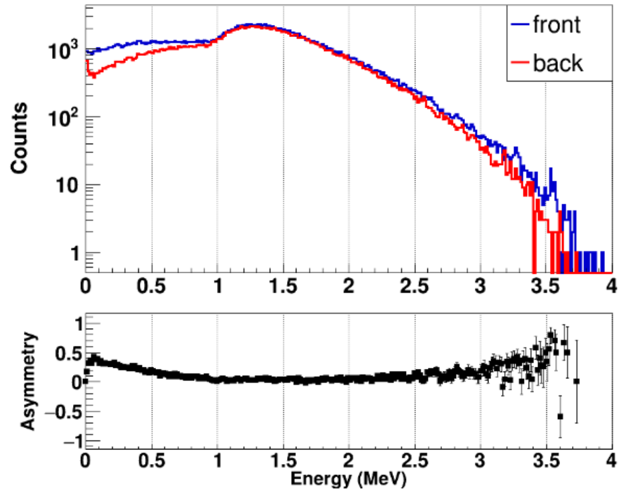

(a) ^{47}K isotope, 2023 geometry

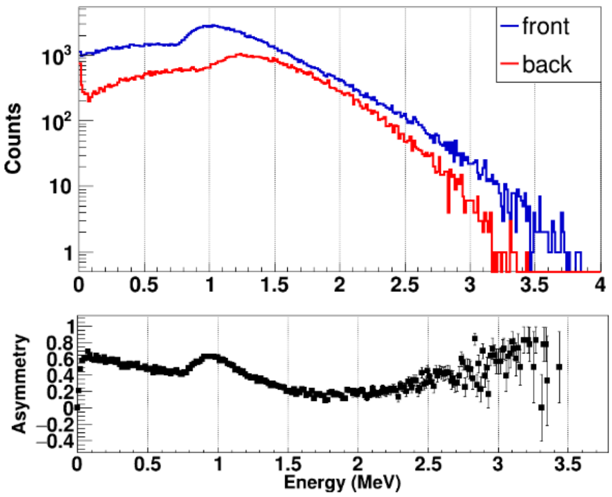

(b) ^{47}K isotope, 2024 geometry

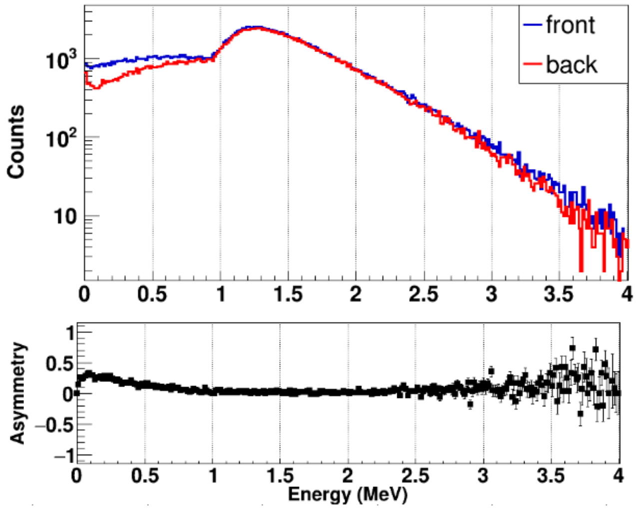

(c) ^{49}K isotope, 2023 geometry

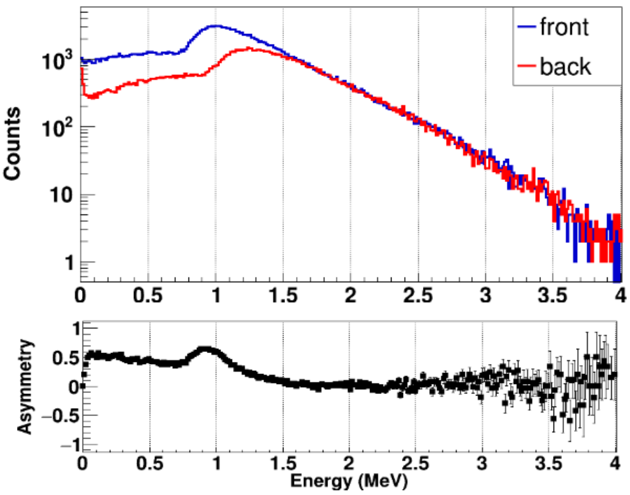

(d) ^{49}K isotope, 2024 geometry

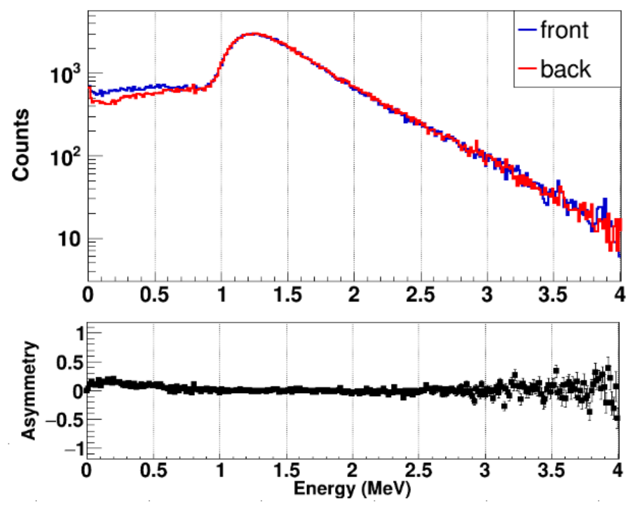

(e) ^{51}K isotope, 2023 geometry

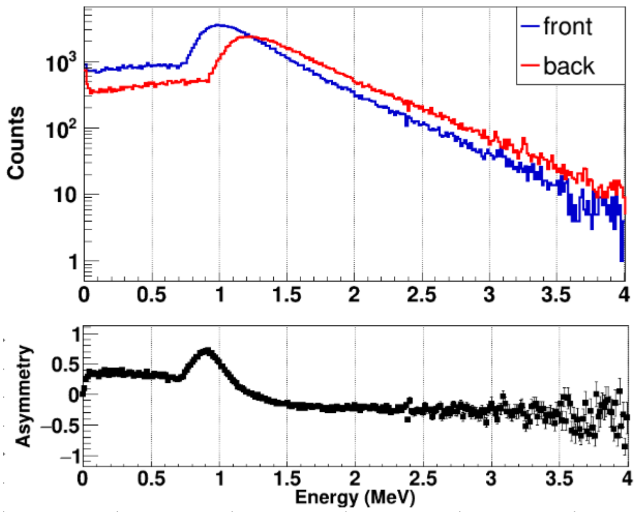

(f) ^{51}K isotope, 2024 geometry

Figure 6: Top panels: The energy deposition as function of β-particle energy in the front and back detectors for 2023 and 2024 geometry. Bottom panels: The instrumental asymmetry as function of energy.

4 Conclusion

In this project, we evaluated the β-particle detection performance of the DeVITO detectors. The instrumental response relevant to radiation asymmetry measurements was investigated by implementing detailed detector and implantation host geometries into the simulation code. The inputs to these simulations were guided by the physics goals of the first DeVITO experiment, focusing on the energy ranges relevant to decay studies of neutron-rich potassium isotopes. Detection efficiency was determined for both mono-energetic electrons and realistic β-particle spectra of ^{47}K, ^{49}K, and ^{51}K. Additionally, the energy deposition of β particles emitted from these three isotopes was studied in both the detector and host crystal volumes. The preliminary results presented above indicate that the detection performance meets the design goals. The DeVITO station is well-suited for studying very neutron-rich nuclei emitting β particles with energies ranging from several to tens of MeV, confirming its capability to measure β-particle emission asymmetries.

References

[1] B. Singh et al. *Nuclear Data Sheets*, 84(3):487, 1998.

[2] H. Miyatake et al. *Phys. Rev. C*, 67:014306, 2003.

[3] M. Kowalska et al. *Journal of Physics G: Nuclear and Particle Physics*, 44(8):084005, 2017.

[4] M. Piersa-Siłkowska et al. Technical report, CERN-INTC-2023-026, INTC-P-662, 2023.

[5] S. Agostinelli et al. *Nuclear Instruments and Methods in Physics*, 506(3):250–303, 2003.

[6] Nucleonica GmbH Online Nuclear Science Applications, accessed August 2024.